arXiv:1306.5256v1 [cond-mat.mes-hall] 21 Jun 2013

Local Ionization Dynamics Traced by Photo-assisted Scanning Tunneling Microscopy: a Theoretical Approach

Michael Schüler,* Yaroslav Pavlyukh, and Jamal Berakdar

Institute for Physics, Martin-Luther University Halle-Wittenberg

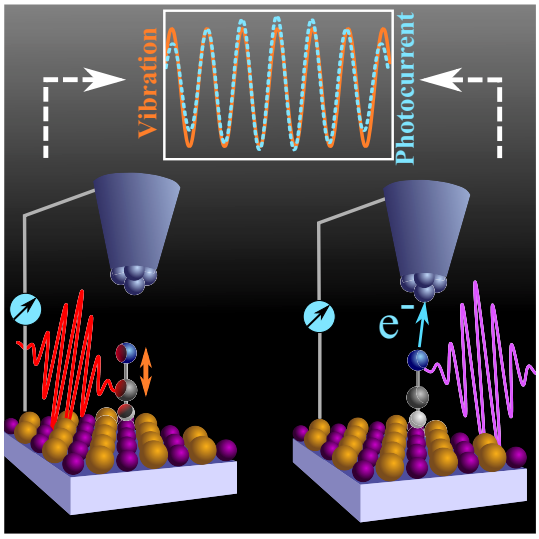
Heinrich-Damerow-Straße 4, 06120 Halle

E-mail: michael.schueler@physik.uni-halle.de

*To whom correspondence should be addressed

Abstract

For tracing the spatiotemporal evolution of electronic systems we suggest and analyze theoretically a setup that exploits the excellent spatial resolution based on scanning tunneling microscopy techniques combined with the temporal resolution of femtosecond pump-probe photoelectron spectroscopy. As an example we consider the laser-induced, local vibrational dynamics of a surface-adsorbed molecule. The photoelectrons released by a laser pulse can be collected by the scanning tip and utilized to access the spatio-temporal dynamics. Our proof-of-principle calculations are based on the solution of the time-dependent Schrödinger equation supported by the *ab initio* computation of the matrix elements determining the dynamics.



Keywords: surface photochemistry, surface vibrations, time-resolved photoemission, photo-assisted STM, Dyson orbital, orbital imaging

The impressive advances made in generating and utilizing sub-femtosecond laser pulses[1–6] for time-resolving the dynamics of electronic systems are paralleled with the fascinating versatility of scanning tunneling microscopy (STM)[7–10] that allows for atomic spatial resolution. STM accesses also spectroscopic information that are related, under certain assumptions, to the local density of states of the probe. The transport through single molecules[11–16] provides, for instance, insight in the analysis and manipulation of the molecular properties like the conformation,[17–19] or the characterization of magnetic systems.[20–22]

To explore the sub-pico second local dynamics, there have been proposals for inducing and probing the electron dynamics by means of focused femtosecond laser pulses applied within the STM context.[23–26] The experimental limitations and issues experienced by earlier attempts (mainly due the thermal expansion of the tip)[23–25] have been shown to be possible to be circumenvented by ultrafast two-photon schemes.[26,27]

We propose in this contribution a new model system that demonstrates the feasibility for tracing the femtosecond dynamics of adsorbed atoms or molecules by means of two-photon[28–30] ultrafast STM-based photoelectron detection. As a concrete example (1), we consider a metal substrate coated with the LiF overlayer, where a single HCN molecule is adsorbed. The LiF layer has the important advantage of a large band gap E_{g} (for the bulk at zero temperature, $E_{\mathrm{g}} = 14.2$ eV, ref.[31]). Provided the ionization energy of adsorbate is smaller than LiF work function, the dynamics of the molecule can be accessed selectively. Furthermore, the strongly ionic character gives rise to a particular strong bonding of the HCN molecule (which also has a large permanent dipole moment of 1.172 a.u.[32,33]) to the surface. Our molecule serves as a test object representing the simplest organic molecule and has some further convenient properties, which will be elucidated by the analysis of the electronic properties.

Our goal is to study the transient vibrational dynamics induced by a infrared (IR) laser pulse (the pump pulse) of moderate intensity and the vibronic coherent motion that can be imaged by utilizing the STM tip for recording the photocurrent (see the (WEO1) for the video illustration). This approach is, strictly speaking, not identical to the STM setup in the tunneling regime. Recent experiments[34] have however demonstrated the feasibility and the potential of the local photoelectron detection with the tip apex, reaching a spatial resolution in range of 5 nm. The photoelectron is released by a second laser pulse (the probe pulse) that ionizes the molecule and is applied at a time delay τ with respect to the pump pulse. We remark that the laser intensities and frequencies are chosen such that only a single electron can be released at a time. The delay before launching a second pump-probe sequence is large enough to allow electrons from the metal substrate to tunnel to the HCN^+ molecule (characteristic time scale in the range of femtoseconds to picoseconds). On

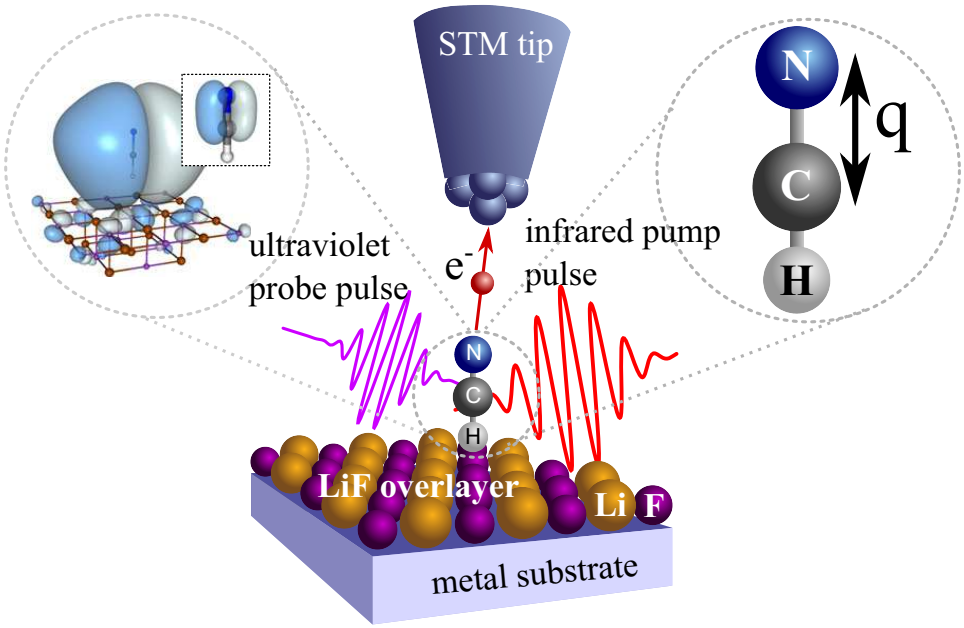


Figure 1: The model system proposed to investigate the local vibrational dynamics of a single HCN molecule adsorbed on the LiF(001) surface. After an infrared (IR) pump pulse has induced the vibrational dynamics, a second laser pulse photo-ionizes the molecule. The released electron collected by a STM tip can then be employed for tracing the transient dynamics.

the other hand, the molecule has to relax to the initial vibrational state (time scale of picoseconds to nanosecond). Considering both of these aspects we estimate the maximal repetition frequency of about 10 MHz for the experiment.

Based on a cluster approach for representing the LiF surface, we have found that the most stable equilibrium configuration of HCN is to stand upright on surface, with the positively charged hydrogen atom directly above a F site (further details in the Supporting Information) by bonding to the surface. The comparison the with cluster computations reveals that the C-N and the H-C stretching modes of the isolated HCN molecule[35] are hardly altered (see Supporting Information). This result is also expected from the chemical point of view due to the strongly ionic character of both subsystems. Similarly, we found that the highest occupied molecular orbital (HOMO) of the HCN molecule (twice degenerated π orbital in the isolated case) is hardly changed by the presence

of the surface (inset in 1) and possesses the same symmetry.

The shape of the HOMO suggests that the excitation of the C-N stretching mode is closely related to contracting or expanding the orbital. As the HOMO strongly influences the photoionization properties, we expect that a particularly clear connection between the vibrational dynamics and the photocurrent can be established when analyzing the C-N stretching eigenmode. We thus choose as the (one-dimensional) vibrational coordinate q the distance between the carbon and the nitrogen atom (inset in 1). The hydrogen atom also participates in the vibration, but with a much smaller amplitude.

For describing the laser-induced vibronic dynamics as well as the photoionization process, we need the q-dependent energy levels. We have computed all the corresponding potential energy surfaces (PESs) within the range of 15 eV from the ground state and accounted only for those states with a nonzero transition matrix element whilst exploiting the dipole selection rules for the case of a linear polarization of the laser field set parallel to the molecule axis (2). The incident laser fields are assumed to enter under small angle such that the components of the polarization perdendicular to the molecule axis can be ignored. Since the molecular dynamics is slow compared to the electronic transitions driven by the probe pulse,we can assume the bond angle to be constant for the photoionization process and thus neglect a transition to PESs associated to a bended conformation of the molecule.[36,37] The computations yield the transitions pathways for the light-molecule interaction: photoionization and the electronic excitation of the neutral system (no contribution to the photocurrent). As both channels influence each other, including the neutral excited states is required for quantitative insights.

We solved the time-dependent Schrödinger equation (TDSE) governing the vibrational dynamics in the presence of the infrared laser field $E(t)$. For the latter we assume a Gaussian form $E(t) = E_0 \exp(-t^2/2T_{\mathrm{IR}}^2)\cos(\omega_{\mathrm{IR}} t)$ with $\omega_{\mathrm{IR}} = 329.2$ meV (this value matches the transition energy from the ground state to the first excited state with respect to the potential $\varepsilon_0(q)$ (2). The corresponding wave length is $\lambda_{\mathrm{IR}} = 3.77$ μm) and $T_{\mathrm{IR}} = 20$ fs. The field amplitude derives from the intensity $I_{\mathrm{IR}} = 1.06 \times 10^{13}$ W/cm^2.

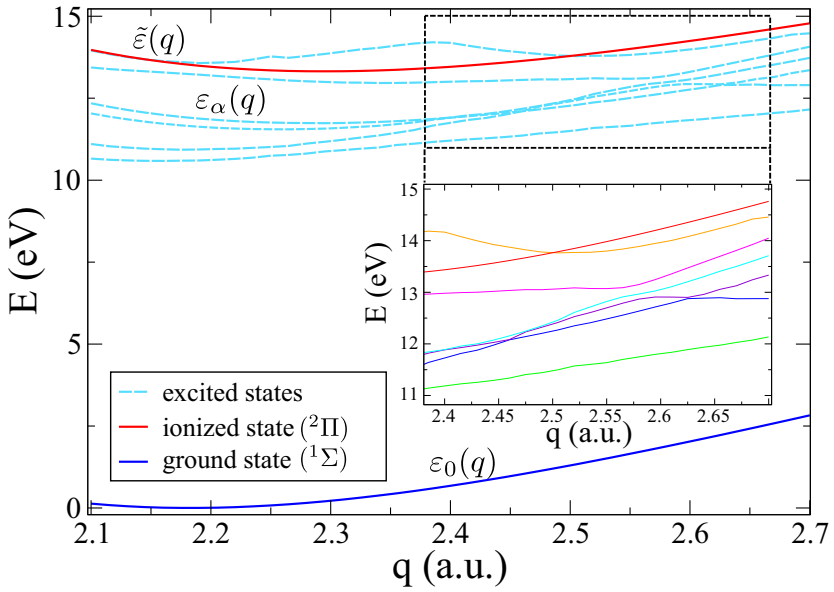


Figure 2: The PESs of the neutral ground state (blue), the neutral excited states (light blue, dashed) and the ground state of HCN^+ (red), as a function of the vibrational coordinate q. The inset magnifies the region where the neutral excited states display energies very close to each other and shows the occurrence of avoided crossings.

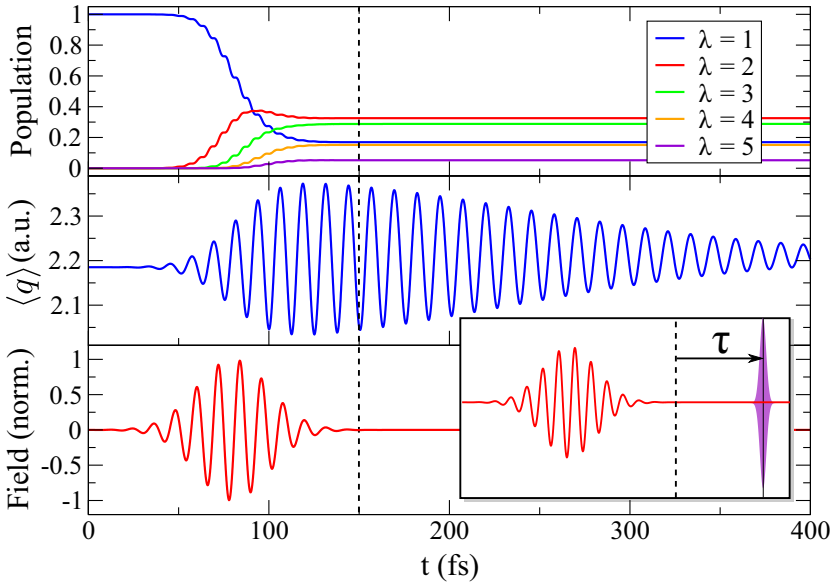


Figure 3: The vibrational dynamics of the HCN molecule in the presence of the infrared laser field (shown in the bottom panel) in terms of the level population (top panel) and the time-dependent expectation value of q (panel in the middle). The inset illustrates the definition of the pump-probe delay τ.

With this specific choice of the parameters the population transfer is primarily induced from the vibronic ground state to the first excited state, but the pulse spectral width due to the short pulse duration may allow higher levels to participate in the dynamics (see 3, top panel, where the states are labeled with the vibrational quantum number λ). The corresponding coherent motion of the wave packet is represented by the time-dependent expectation value of q (the middle panel in 3), displaying an oscillation with an amplitude of 10 % around the equilibrium value. The laser field $E(t)$ is shown in the bottom panel in 3.

To unravel how the vibronic wave packet characterized in 3 can be traced in the quantities of interest, we analyzed the respective many-body TDSE and derived a coupled set of equations including the bound-state dynamics and the release and propagation of exactly one photoelectron to the tip in the presence of the probe pulse. The assume an ultraviolet (UV) Gaussian-shaped laser pulse (central wave length $\lambda_{\mathrm{UV}} = 100$ nm, peak intensity $I_{\mathrm{UV}} = 3.5 \times 10^{14}$ W cm^{-2} and pulse length $T_{\mathrm{UV}} = 1.97$ fs FWHH). A detailed derivation is provided in the Supporting Information, along with the necessary additional approximations: (i) we ignore correlation effects of the photoelectron with the remaining ones, (ii) ignore second-order overlap terms of well-localized orbitals with the continuum wave function of the released electron and (iii) we employ the Born-Oppenheimer (BO) approximation.[38] For the latter, we spend a few words more on the justification for our model system. Since the diabatic coupling matrix elements of the electronic wave functions sandwiching the derivatives with respect to the vibrational coordinate are related to the velocity (the kinetic energy) of the nuclei (slow on the electronic time scale) divided by the energy level spacing of the states, these matrix elements play only a minor role as long as the electronic levels are well-separated. This is, e. g., the case for the ground state in 2, but not for the excited states. However, the physical picture of the slow nuclei implies that the diabatic coupling elements have only a minor influence on the short-time dynamics, i. e. when restricting the pulse length of the probing electrical field to a time scale small compared to the characteristic time scale for the vibrations, the BO approximation is still valid. This assumption is tolerable in view of the fact that $T_{\mathrm{UV}}/T_{\mathrm{vib}} \sim 0.1$. We furthermore specialize to the scenario sketched in 4(a), i. e. we assume that no transitions between the neutral

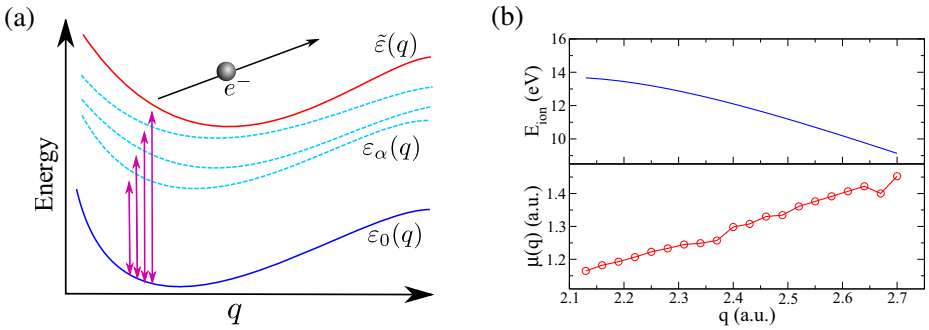


Figure 4: (a) The simplifying model for the ionization process: the spectral properties of the laser field only allow for the transitions from the ground state to the excited states or the ionic ground state (indicated by the purple double arrows). (b) The q-dependent ionization energy and the momentum-integrated transition strength.

excited state occur, which is ensured by the spectral properties of the probe pulse

Apart from the approximations stated above, our treatment of the coupled population dynamics of the involved electronic states of the neutral molecule the released electron is exact. The photoelectron wave function is represented on a real-space grid, i. e. it does need to be constructed invoking additional approximations. The charge interaction of the photoelectron with the ionized molecule and the time-dependent laser field is taken into account, as well.

The experimentally measurable quantity is the photoionization current. Our studies have elucidated that the key quantity connecting the vibrations in the ground state PES $\varepsilon_0(q)$ and the photocurrent is the transition matrix element of the Dyson orbital with the photoelectron wave function. The Dyson orbital ϕ_0[39,40] is defined as the overlap of the $N-$electron wave function with the $(N-1)-$electron wave function of the ionized system. We computed ϕ_0 by approximating the dominant configurations of the ground states of both the neutral and the ionized molecule by the Hartree-Fock determinants. The (expected) result reveals that this Dyson orbital overlaps by about 90 % with the HOMO. Since the C-N stretching vibration directly contracts or expands the HOMO, we expect an almost linear dependence of the transition strength on the vibrational coordinate. This scenario is supported by the calculation of the transition matrix element (integrated over the momentum of the photoelectron), depicted in 4.

Solving the corresponding time-dependent Schrödinger equation yields the photoelectron wave

function and thus the measurable current density **j**. For the pump-probe experiment, the time-integrated current (i. e. a probability) rather than the actual time-dependent current **j** contains the desired information. Taking the projection in the direction of the tip yields the spatio-resolved probability P of detecting a photoelectron in a plane parallel to the surface and entails the information on the initial vibrational wave packet. We consider a plane with a distance of $d = 4.5$ Å above the nitrogen atom (x-y plane) and compute the detection probability as a function of the position and the time delay τ between the pump and the probe pulse. For $\tau = 0$ the maximum of the UV pulse being centered at $t = 150$ fs (see inset in 3(b)).

The spatial dependence of P is shown in 5(a). Since the photoelectron primarily originates from the Dyson orbital ϕ_0, we can expect that the spatial structure of the detection probability in the detection plane is related to a cut through the x-y plane of ϕ_0. At this point, we have to take for the degeneracy of the HOMO and add the probability contributions according to the two orientations of the Dyson orbital, resulting in a radially symmetric spatial dependence. Interestingly, the probability displays a minimum directly above the molecule, as the Dyson orbital has a nodal plane along the molecule axis. We infer thus that the dependence of P on x and y yields a probability map which is closely related to viewing the Dyson orbital "from above".

We proceed by fixing x and y such that the detection probability is maximal and study the dependence on τ. As we have already discussed, we expect an approximately linear mapping of the coherent vibrational dynamics to the detection probability for two reasons: the dependence of (i) the ionization energy and (ii) the transition strength to the continuum on q is almost linear. The result is presented in 5(b), where the expectation value of the vibrational coordinate is also shown for a comparison. Both curves are very similar though some higher-frequency components occur evidencing non-linear contributions. As an outcome of this study, animation (WEO2) illustrates the time evolution of the vibronic wave packet simultaneously with the τ-dependent detection probability (spatially resolved along the x axis).

In conclusion, we suggested theoretically a novel experimental setup to access the spatio-temporal dynamics of adsorbates. The proposal is based on a combination of pump-probe tech-

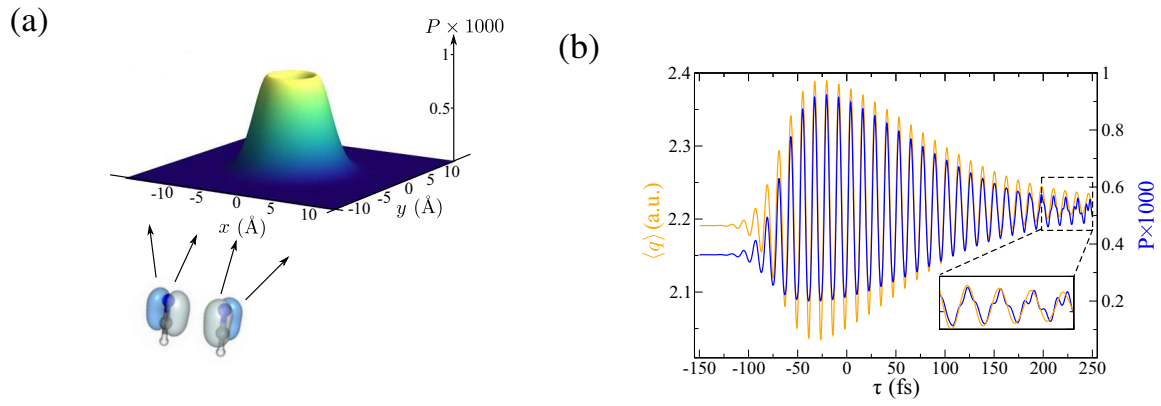


Figure 5: (a) The spatial dependence of the detection probability P in the shifted x-y plane placed ~ 4.5 Å above the molecule, for fixed $\tau = -150$ fs. Both possible orientation directions of the degenerated Dyson orbital ϕ_0 are taken into account. (b) The comparison of the expectation value $\langle q \rangle$ from 3 with the detection probability P, as a function of the pump-probe delay τ. The point in space for the detection is the same plane as in (a), such that P has the maximal amplitude.

niques with a local detection scheme. We illustrated the model by studying explicitly a sample consisting of a HCN molecule adsorbed on a LiF overlayer deposited on a metal substrate. We studied how the molecule is adsorbed on the surface and find that the vibrational as well as the electronic properties are hardly altered. The proposed setup involved (i) the excitation of a coherent vibronic wave packet due to an infrared pump pulse, and (ii) the photoionization of the adsorbed molecule by an ultraviolet probe pulse. (iii) The photoelectrons are detected by the STM tip. We demonstrated by a proof-of-principle calculation how the vibronic wave packet can be mapped onto a probability P detected by the STM tip. The tip position yields the spatial dependence and can be exploited to image the involved orbitals. The temporal dependence with respect to the pump-probe delay τ yields a measurable signal which closely resembles the time-dependent expectation value of the vibrational coordinate q, characterizing the coherent dynamics. While our proof-of-principle study concentrates on a rather simple molecule, a generalization to more complex systems is conceptionally straight forward. The combination of spatial and temporal resolution potentially coalesces in, e. g., probing relaxation and decoherence processes or photo-induced

conformation switching on single molecules in the time domain.

Theoretical methods

All structure computations have been carried out using the GAUSSIAN 03 code. Details (method, basis set) for each of the steps are provided in the Supporting Information. For the time-propagation of the photoelectron wave function we employed a fourth-order Runge-Kutta scheme and discretized the spatial derivatives to the fourth order.

Acknowledgement

This research is supported financially by the DFG through SFB 762.

Associated content

Web Enhanced Object 1 (WEO1). Schematic video of the model system and the setup. Available in the HTML version of the paper.

Web Enhanced Object 2 (WEO2). Animation of the time-delay dependence of the vibrational wave-packet dynamics synchronized with the detection probability. Available in the HTML version of the paper.

Supporting Information Availabe:. Details for the computations of the vibrational modes and the orbitals of the surface-molecule system, for calculating the PESs and the derivation of Schrödinger equations for the photoemission. Available free of charge via the Internet at `http://pubs.acs.org`.

References

(1) Goulielmakis, E.; Schultze, M.; Hofstetter, M.; Yakovlev, V. S.; Gagnon, J.; Uiberacker, M.; Aquila, A. L.; Gullikson, E. M.; Attwood, D. T.; Kienberger, R.; Krausz, F.; Kleineberg, U. Single-Cycle Nonlinear Optics. *Science* **2008**, *320*, 1614–1617.

(2) Schultze, M.; Fieß, M.; Karpowicz, N; Gagnon, J.; Korbman, M; Hofstetter, M.; Neppl, S.; Cavalieri, A. L.; Komninos, Y.; Mercouris Th. et al. Delay in Photoemission. *Science* **2010**, *328*, 1658–1662.

(3) Haessler, S.; Caillat, J.; Boutu, W.; Giovanetti-Teixeira, C.; Ruchon, T.; Auguste, T.; Diveki, Z.; Breger, P.; Maquet, A.; Carré, B.; Taïeb, R.; Salières, P. Attosecond Imaging of Molecular Electronic Wavepackets. *Nature Phys.* **2010**, *6*, 200–206.

(4) Shafir, D.; Mairesse, Y.; Villeneuve, D. M.; Corkum, P. B.; Dudovich, N. Atomic Wavefunctions Probed through Strong-Field Light-Matter Interaction. *Nature Phys.* **2009**, *5*, 412–416.

(5) Krausz, F.; Ivanov, M. Attosecond Physics. *Rev. Mod. Phys.* **2009**, *81*, 163–234.

(6) Cavalieri, A. L.; Müller, N.; Uphues, Th.; Yakovlev, V. S.; Baltuška, A.; Horvath, B.; Schmidt, B.; Blümel, L.; Holzwarth, R.; Hendel, S. et al. Attosecond Spectroscopy in Condensed Matter. *Nature* **2007**, *449*, 1029–1032.

(7) Oka, H.; Ignatiev, P. A.; Wedekind, S.; Rodary, G.; Niebergall, L.; Stepanyuk, V. S.; Sander, D.; Kirschner, J. Spin-Dependent Quantum Interference Within a Single Magnetic Nanostructure. *Science* **2010**, *327*, 843–846.

(8) Wiesendanger, R. Spin Mapping at the Nanoscale and Atomic Scale. *Rev. Mod. Phys.* **2009**, *81*, 1495–1550.

(9) Fu, Y.-S.; Schwöbel, J.; Hla, S.-W.; Dilullo, A.; Hoffmann, G.; Klyatskaya, S.; Ruben, M.; Wiesendanger, R. Reversible Chiral Switching of Bis(phthalocyaninato) Terbium(III) on a Metal Surface. *Nano Lett.* **2012**, *12*, 3931–3935.

(10) Schwöbel, J.; Fu, Y.; Brede, J.; Dilullo, A.; Hoffmann, G.; Klyatskaya, S.; Ruben, M.; Wiesendanger, R. Real-Space Observation of Spin-Split Molecular Orbitals of Adsorbed Single-Molecule Magnets. *Nature Communications* **2012**, *3*, 953.

(11) Müllegger, S.; Schöfberger, W.; Rashidi, M.; Reith, L. M.; Koch, R. Spectroscopic STM Studies of Single Gold(III) Porphyrin Molecules. *J. Am. Chem. Soc.* **2009**, *131*, 17740–17741.

(12) Katano, S.; Kim, Y.; Kagata, Y.; Kawai, M. Single-Molecule Vibrational Spectroscopy and Inelastic-Tunneling-Electron-Induced Diffusion of Formate Adsorbed on Ni(110). *J. Phys. Chem. C* **2010**, *114*, 3003–3007.

(13) Burema, S. R.; Bocquet, M.-L. Resonance Charges to Encode Selection Rules in Inelastic Electron Tunneling Spectroscopy. *J. Phys. Chem. Lett.* **2012**, *3*, 3007–3011.

(14) Jiang, N.; Foley, E. T.; Klingsporn, J. M.; Sonntag, M. D.; Valley, N. A.; Dieringer, J. A.; Seideman, T.; Schatz, G. C.; Hersam, M. C.; Van Duyne, R. P. Observation of Multiple Vibrational Modes in Ultrahigh Vacuum Tip-Enhanced Raman Spectroscopy Combined with Molecular-Resolution Scanning Tunneling Microscopy. *Nano Lett.* **2012**, *12*, 5061–5067.

(15) Zhao, J.; Feng, M.; Yang, J.; Petek, H. The Superatom States of Fullerenes and Their Hybridization into the Nearly Free Electron Bands of Fullerites. *ACS Nano* **2009**, *3*, 853–864.

(16) Jorn, R.; Zhao, J.; Petek, H.; Seideman, T. Current-Driven Dynamics in Molecular Junctions: Endohedral Fullerenes. *ACS nano* **2011**, *5*, 7858–7865.

(17) Braun, K.-F.; Hla, S.-W. Probing the Conformation of Physisorbed Molecules at the Atomic Scale Using STM Manipulation. *Nano Lett.* **2005**, *5*, 73–76.

(18) Alemani, M.; Peters, M. V.; Hecht, S.; Rieder, K.-H.; Moresco, F.; Grill, L. Electric Field-Induced Isomerization of Azobenzene by STM. *J. Am. Chem. Soc.* **2006**, *128*, 14446–14447.

(19) Kuck, S.; Hoffmann, G.; Bröring, M.; Fechtel, M.; Funk, M.; Wiesendanger, R. "Naked" Iron-5,10,15-triphenylcorrole on Cu(111): Observation of Chirality on a Surface and Manipulation of Multiple Conformational States by STM. *J. Am. Chem. Soc.* **2008**, *130*, 14072–14073.

(20) Loth, S.; Etzkorn, M.; Lutz, C. P.; Eigler, D. M.; Heinrich, A. J. Measurement of Fast Electron Spin Relaxation Times with Atomic Resolution. *Science* **2010**, *329*, 1628–1630.

(21) Loth, S.; Baumann, S.; Lutz, C. P.; Eigler, D. M.; Heinrich, A. J. Bistability in Atomic-Scale Antiferromagnets. *Science* **2012**, *335*, 196–199.

(22) Robles, R.; Lorente, N.; Isshiki, H.; Liu, J.; Katoh, K.; Breedlove, B. K.; Yamashita, M.; Komeda, T. Spin Doping of Individual Molecules by Using Single-Atom Manipulation. *Nano Lett.* **2012**, *12*, 3609–3612.

(23) Pfeiffer, W.; Sattler, F.; Vogler, S.; Gerber, G.; Grand, J. Y.; Möller, R. Photoelectron Emission in Femtosecond Laser Assisted Scanning Tunneling Microscopy. *Appl. Phys. B* **1997**, *64*, 265–268.

(24) Gerstner, V.; Knoll, A.; Pfeiffer, W.; Thon, A.; Gerber, G. Femtosecond Laser Assisted Scanning Tunneling Microscopy. *J. Appl. Phys.* **2000**, *88*, 4851–4859.

(25) Grafstrom, S. Photoassisted Scanning Tunneling Microscopy. *J. Appl. Phys.* **2002**, *91*, 1717–1754.

(26) Lee, J.; Perdue, S. M.; Whitmore, D.; Apkarian, V. A. Laser-Induced Scanning Tunneling Microscopy: Linear Excitation of the Junction Plasmon. *J. Chem. Phys.* **2010**, *133*, 104706.

(27) Dolocan, A.; Acharya, D. P.; Zahl, P.; Sutter, P.; Camillone, N. Two-Color Ultrafast Photoexcited Scanning Tunneling Microscopy. *J. Phys. Chem. C* **2011**, *115*, 10033–10043.

(28) Knoesel, E.; Hertel, T.; Wolf, M; Ertl, G. Femtosecond Dynamics of Electronic Excitations of Adsorbates Studied by Two-Photon Photoemission Pulse Correlation: CO/Cu(111). *Chem. Phys. Lett.* **1995**, *240*, 409–416.

(29) Gruebele, M.; Zewail, A. H. Femtosecond Wave Packet Spectroscopy: Coherences, the Potential, and Structural Determination. *J. Chem. Phys.* **1993**, *98*, 883.

(30) Petel, H.; Ogawa, S. SURFACE FEMTOCHEMISTRY: Observation and Quantum Control of Frustrated Desorption of Alkali Atoms from Noble Metals. *Ann. Rev. Phys. Chem.* **2002**, *53*, 507–531.

(31) Tran, F.; Blaha, P. Accurate Band Gaps of Semiconductors and Insulators with a Semilocal Exchange-Correlation Potential. *Phys. Rev. Lett.* **2009**, *102*, 226401.

(32) Thomas, J. R.; DeLeeuw, B. J.; Vacek, G.; Crawford, T. D.; Yamaguchi, Y.; Schaefer, H. F. The Balance between Theoretical Method and Basis Set Quality: A Systematic Study of Equilibrium Geometries, Dipole Moments, Harmonic Vibrational Frequencies, and Infrared Intensities. *J. Chem. Phys.* **1993**, *99*, 403.

(33) Bündgen, P.; Grein, F.; Thakkar, A. J. Dipole and quadrupole moments of small molecules. An ab initio Study using Perturbatively Corrected, Multi-Reference, Configuration Interaction Wave Functions. *J. Mol. Struct.* **1995**, *334*, 7–13.

(34) Yu, P.; Kirschner, J. Nanoscale Imaging of Photoelectrons using an Atomic Force Microscope. *Appl. Phys. Lett.* **2013**, *102*, 063111.

(35) Mellau, G. C. The ν_1 band system of HNC. *J. Mol. Spectrosc.* **2010**, *264*, 2–9.

(36) Schwenzer, G. M.; O'Neil, S. V.; Schaefer III, H. F.; Baskin, C. P.; Bender, C. F. Geometries of the Excited Electronic States of HCN. *J. Chem. Phys.* **1974**, *60*, 2787.

(37) Nayak, M. K.; Chaudhuri, R. K.; Krishnamachari, S. N. L. Theoretical Study on the Excited States of HCN. *J. Chem. Phys.* **2005**, *122*, 184323.

(38) Drake, G. W. F. *Springer Handbook of Atomic, Molecular, and Optical Physics*; Springer: New York, USA; 2005.

(39) Melania Oana, C.; Krylov, A. I. Dyson Orbitals for Ionization from the Ground and Electronically Excited States Within Equation-of-Motion Coupled-Cluster Formalism: Theory, Implementation, and Examples. *J. Chem. Phys.* **2007**, *127*, 234106.

(40) Oana, C. M.; Krylov, A. I. Cross Sections and Photoelectron Angular Distributions in Photodetachment from Negative Ions using Equation-of-Motion Coupled-Cluster Dyson orbitals. *J. Chem. Phys.* **2009**, *131*, 124114.